

Numerical methods for computing the ground state of spin-1 Bose-Einstein condensates in a uniform magnetic field

Fong Yin Lim and Weizhu Bao*

Department of Mathematics and Center for Computational Science and Engineering,
National University of Singapore, Singapore 117543

(Received 26 December 2007; revised manuscript received 22 September 2008; published 30 December 2008)

We propose efficient and accurate numerical methods for computing the ground-state solution of spin-1 Bose-Einstein condensates subjected to a uniform magnetic field. The key idea in designing the numerical method is based on the normalized gradient flow with the introduction of a third normalization condition, together with two physical constraints on the conservation of total mass and conservation of total magnetization. Different treatments of the Zeeman energy terms are found to yield different numerical accuracies and stabilities. Numerical comparison between different numerical schemes is made, and the best scheme is identified. The numerical scheme is then applied to compute the condensate ground state in a harmonic plus optical lattice potential, and the effect of the periodic potential, in particular to the relative population of each hyperfine component, is investigated through comparison to the condensate ground state in a pure harmonic trap.

DOI: [10.1103/PhysRevE.78.066704](https://doi.org/10.1103/PhysRevE.78.066704)

PACS number(s): 02.60.-x, 03.75.Mn, 03.75.Hh, 03.75.Lm

I. INTRODUCTION

Since the experimental realizations of Bose-Einstein condensation (BEC) in alkali-metal atomic gases in 1995 [1–3], extensive theoretical and experimental studies have been stimulated to investigate various novel phenomena of the condensates. In earlier BEC experiments, the atoms were confined in a magnetic trap, in which the spin degree of freedom is frozen. The particles are described by a scalar model, and the wave function of the particles is governed by the Gross-Pitaevskii equation (GPE) within the mean-field approximation [4–6]. In recent years, experimental achievements of spin-1 and spin-2 condensates in optical traps [7–12] have offered new regimes to study a rich variety of quantum phenomena which are generally absent in a single-component condensate. In contrast to a single-component BEC, a spin- F BEC is described by the generalized coupled GPEs which consist of $2F+1$ equations, each governing one of the $2F+1$ hyperfine states ($m_F = -F, -F+1, \dots, F-1, F$) within the mean-field approximation. The formulation was first carried out by Ho [13] and Ohmi and Machida [14] for spin-1 condensates and Ciobanu *et al.* [15], and Ueda and Kaoshi [16] for spin-2 condensates.

In the effort at exploring the rich properties of spinor dynamics, various theoretical studies—e.g., coreless vortices [17], quantum tunneling phenomena in double-well potentials [18], interactions of soliton solutions [19], the effect of finite temperature in the context of the Bogoliubov–de Gennes framework [20], etc.—have been carried out to date by several authors. From a numerical point of view, the simulation of spinor dynamics requires the preparation of condensates in a certain initial state, which is usually represented by the condensate ground state under a certain experimental setup. In their first achievement of spin-1 BEC in ^{23}Na , Stenger *et al.* [7] reported the ground-state phase dia-

gram of a uniform spin-1 condensate in the Thomas-Fermi regime, with the existence of an external magnetic field. Recently, Murata *et al.* [21] also studied the broken axisymmetry phase of spin-1 ferromagnetic condensates subjected to a certain magnetic field. In numerical studies of spin-1 BEC, Zhang *et al.* [22] reported the ground-state phase diagram for both ^{87}Rb and ^{23}Na confined in a harmonic trap subjected to a uniform magnetic field. The imaginary-time method with several adjustable parameters was applied to solve the three-component GPEs under the conservation of total mass and total magnetization.

The imaginary-time method, which is mathematically justified by the normalized gradient flow, was long known to be widely used to compute the ground state of single-component condensates [23–25]. If the method is directly extended to spin-1 BEC, the two normalization conditions, conservation of total mass and conservation of total magnetization, are insufficient to determine the three normalization constants in the normalization step. To solve the problem, Bao and Lim [26] introduced a third normalization condition based on the relation between the chemical potentials of the three hyperfine components. The three normalization constants can then be determined explicitly, and the ground state can be computed in a determinate and efficient way. The aim of this paper is to extend the method proposed in Ref. [26] to take the external magnetic field into account as well as to present its modification to attain better numerical stability in computing the spin-1 condensate ground state subjected to a uniform magnetic field. Two different ways of incorporating the uniform magnetic field in the normalized gradient flow will be presented. Comparison of the numerical accuracies of the two numerical methods, combined with the spectrally accurate sine-pseudospectral discretization [25], will be made through various numerical examples. The best numerical scheme will be identified and applied to compute the mean-field ground state of a spin-1 BEC in an optical lattice potential. The effect of the periodic potential as well as the effect of the mean-field interaction, to the relative population

*bao@math.nus.edu.sg

of each spinor component, as compared to the condensate ground state in a pure harmonic trap, will also be investigated.

The paper is organized as follows. In Sec. II, the coupled GPEs for a spin-1 condensate in an external magnetic field will be reviewed. In Sec. III, we will introduce modified numerical methods for computing the spin-1 BEC ground state in a uniform magnetic field. Two different treatments of the Zeeman energy terms will be considered. In Sec. IV, the numerical methods are combined with different discretization techniques. The numerical accuracies and stabilities of different combinations will be studied through examples and the best combination will be identified. In Sec. V, we will show the application of the method to simulate the spin-1 BEC ground state with ferromagnetic interaction and antiferromagnetic interaction, respectively. Finally, concluding remarks will be drawn in Sec. VI.

II. MODEL

At a temperature much lower than the critical temperature T_c , the three-component wave function $\Psi(\mathbf{x}, t) = (\psi_1(\mathbf{x}, t), \psi_0(\mathbf{x}, t), \psi_{-1}(\mathbf{x}, t))^T$, which gives the state of a spin-1 BEC subjected to a uniform external magnetic field B , is described by the coupled Gross-Pitaevskii equations (CGPEs) [13,14,22]

$$i\hbar\partial_t\psi_1 = [H + E_1 + c_0n + c_2(n_1 + n_0 - n_{-1})]\psi_1 + c_2\bar{\psi}_{-1}\psi_0^2, \quad (1)$$

$$i\hbar\partial_t\psi_0 = [H + E_0 + c_0n + c_2(n_1 + n_{-1})]\psi_0 + 2c_2\psi_{-1}\bar{\psi}_0\psi_1, \quad (2)$$

$$i\hbar\partial_t\psi_{-1} = [H + E_{-1} + c_0n + c_2(n_{-1} + n_0 - n_1)]\psi_{-1} + c_2\psi_0^2\bar{\psi}_1, \quad (3)$$

where $H = -\frac{\hbar^2}{2m}\nabla^2 + V(\mathbf{x})$ is the single-particle Hamiltonian and $V(\mathbf{x})$ is a spin-independent trapping potential. When a harmonic trap is considered, $V(\mathbf{x}) = \frac{m}{2}(\omega_x^2x^2 + \omega_y^2y^2 + \omega_z^2z^2)$, where ω_x , ω_y , and ω_z are the trapping frequencies in the x , y , and z directions. $n_l(\mathbf{x}, t) = |\psi_l(\mathbf{x}, t)|^2$ is the spatial density of the hyperfine spin component $m_F = l$ ($l = -1, 0, 1$), and $n = n_1 + n_0 + n_{-1}$ is the total density. $c_0 = \frac{4\pi\hbar^2}{3m}(a_0 + 2a_2)$ characterizes the spin-independent mean-field interaction (positive for repulsive interaction and negative for attractive interaction), while $c_2 = \frac{4\pi\hbar^2}{3m}(a_2 - a_0)$ characterizes the spin-exchange interaction (negative for ferromagnetic interaction and positive for antiferromagnetic interaction) with a_0 (a_2) the s -wave scattering length for a scattering channel of total hyperfine spin 0 (spin 2). E_l ($l = -1, 0, 1$) is the Zeeman energy of spin component $m_F = l$ in the uniform magnetic field. Two parameters playing important roles in the ground-state phase diagram as well as the dynamics of spin-1 condensates are the linear Zeeman energy [7,27,28]

$$p_0 = \frac{1}{2}(E_1 - E_{-1}) \approx -\frac{\mu_B B}{2} \quad (4)$$

and the quadratic Zeeman energy

$$q_0 = \frac{1}{2}(E_1 + E_{-1} - 2E_0) \approx \frac{\mu_B^2 B^2}{4E_{\text{hfs}}}. \quad (5)$$

The right-hand sides of (4) and (5) are obtained when the Breit-Rabi formula is applied. μ_B is the Bohr magneton, and E_{hfs} is the hyperfine splitting.

In order to minimize any possible numerical error that can be caused by large Zeeman energy when (1)–(3) are solved numerically, we shift the energy level and set the zero energy to be E_0 , which is equivalent to replacing $\psi_l \rightarrow \psi_l \exp(-\frac{iE_0 t}{\hbar})$ in (1)–(3). Furthermore, by introducing the dimensionless variables $t \rightarrow t/\omega_m$ with $\omega_m = \min\{\omega_x, \omega_y, \omega_z\}$, $\mathbf{x} \rightarrow \mathbf{x}a_s$ with $a_s = \sqrt{\frac{\hbar}{m\omega_m}}$, $\psi_l \rightarrow \sqrt{N}\psi_l/a_s^{3/2}$ ($l = -1, 0, 1$), with N being the total number of particles in the system, the dimensionless CGPEs are obtained from (1)–(3) as [26,29]

$$i\partial_t\psi_1 = [H + q + p + \beta_n n + \beta_s(n_1 + n_0 - n_{-1})]\psi_1 + \beta_s\bar{\psi}_{-1}\psi_0^2, \quad (6)$$

$$i\partial_t\psi_0 = [H + \beta_n n + \beta_s(n_1 + n_{-1})]\psi_0 + 2\beta_s\psi_{-1}\bar{\psi}_0\psi_1, \quad (7)$$

$$i\partial_t\psi_{-1} = [H + q - p + \beta_n n + \beta_s(n_{-1} + n_0 - n_1)]\psi_{-1} + \beta_s\psi_0^2\bar{\psi}_1, \quad (8)$$

where $H = -\frac{1}{2}\nabla^2 + V(\mathbf{x})$ and the dimensionless harmonic trapping potential $V(\mathbf{x}) = \frac{1}{2}(\gamma_x^2 x^2 + \gamma_y^2 y^2 + \gamma_z^2 z^2)$ with $\gamma_x = \frac{\omega_x}{\omega_m}$, $\gamma_y = \frac{\omega_y}{\omega_m}$, and $\gamma_z = \frac{\omega_z}{\omega_m}$. The dimensionless mean-field and spin-exchange interaction terms are now given by $\beta_n = \frac{Nc_0}{a_s^3\hbar\omega_m} = \frac{4\pi N(a_0 + 2a_2)}{a_s}$ and $\beta_s = \frac{Nc_2}{a_s^3\hbar\omega_m} = \frac{4\pi N(a_2 - a_0)}{a_s}$, while the linear and quadratic Zeeman terms are scaled according to $p = \frac{p_0}{\hbar\omega_m}$ and $q = \frac{q_0}{\hbar\omega_m}$. Three conserved quantities associated with (6)–(8) are the normalization of the wave function

$$N(\Psi(\cdot, t)) := \|\Psi(\cdot, t)\|^2 = \int \sum_{l=-1}^1 |\psi_l(\mathbf{x}, t)|^2 d\mathbf{x} = 1, \quad (9)$$

the total magnetization

$$M(\Psi(\cdot, t)) := \int [|\psi_1(\mathbf{x}, t)|^2 - |\psi_{-1}(\mathbf{x}, t)|^2] d\mathbf{x} = M, \quad (10)$$

and the energy per particle

$$E(\Psi(\cdot, t)) = \int \left\{ \sum_{l=-1}^1 \left(\frac{1}{2} |\nabla\psi_l|^2 + V(\mathbf{x})n_l \right) + \frac{\beta_n}{2} n_0^2 + \frac{\beta_n + \beta_s}{2} [n_1^2 + n_{-1}^2 + 2n_0(n_1 + n_{-1})] + (\beta_n - \beta_s)n_1n_{-1} + \beta_s(\bar{\psi}_{-1}\psi_0^2\bar{\psi}_1 + \psi_{-1}\bar{\psi}_0^2\psi_1) + (q + p)n_1 + (q - p)n_{-1} \right\} d\mathbf{x}. \quad (11)$$

The ground state of a spin-1 BEC, $\Phi_g(\mathbf{x})$, is given by the minimizer of the energy functional (11) subjected to constraints (9) and (10)—i.e.,

Find $(\Phi_g \in S)$ such that

$$E_g := E(\Phi_g) = \min_{\Phi \in S} E(\Phi), \quad (12)$$

where the nonconvex set S is defined as

$$S = \left\{ \begin{aligned} &\Phi = (\phi_1, \phi_0, \phi_{-1})^T \|\Phi\| = 1, \\ &\int [|\phi_1(\mathbf{x})|^2 - |\phi_{-1}(\mathbf{x})|^2] d\mathbf{x} = M, \quad E(\Phi) < \infty \end{aligned} \right\}. \quad (13)$$

It is easy to show that the ground state is also the lowest-energy solution of the time-independent CGPEs

$$\mu_1 \phi_1 = [H + q + p + \beta_n n + \beta_s(n_1 + n_0 - n_{-1})] \phi_1 + \beta_s \bar{\phi}_{-1} \phi_0^2, \quad (14)$$

$$\mu_0 \phi_0 = [H + \beta_n n + \beta_s(n_1 + n_{-1})] \phi_0 + 2\beta_s \phi_{-1} \bar{\phi}_0 \phi_1, \quad (15)$$

$$\mu_{-1} \phi_{-1} = [H + q - p + \beta_n n + \beta_s(n_{-1} + n_0 - n_1)] \phi_{-1} + \beta_s \phi_0^2 \bar{\phi}_1. \quad (16)$$

Here μ_1 , μ_0 , and μ_{-1} are the chemical potentials of the three components and they satisfy

$$\mu_1 = \mu + \lambda, \quad \mu_0 = \mu, \quad \mu_{-1} = \mu - \lambda, \quad (17)$$

with μ and λ being the Lagrange multipliers introduced to the free-energy functional to conserve N and M , respectively. The relation between the chemical potentials as given by

$$\mu_1 + \mu_{-1} = 2\mu_0 \quad (18)$$

plays the key role in the derivation of the third normalization constant for the normalized gradient flow in computing the ground-state solution [26].

III. NUMERICAL METHOD

Since p and q are constants, it is straightforward to apply the normalized gradient flow in Ref. [26] for computing the spin-1 BEC ground state in a uniform magnetic field. However, the linear Zeeman term is always much greater than the quadratic Zeeman—term, i.e., $p \gg q$ —and it causes high instability in the numerical scheme. The numerical scheme does not converge for almost all physically realistic parameter values. For this reason, we have to modify the numerical scheme in Refs. [26,29] for the computation.

We first construct the continuous normalized gradient flow (CNGF) for a spin-1 BEC in a uniform magnetic field:

$$\begin{aligned} \partial_t \phi_1 = & -[H + \beta_n n + \beta_s(n_1 + n_0 - n_{-1})] \phi_1 - \beta_s \bar{\phi}_{-1} \phi_0^2 \\ & + \{\mu_\Phi(t) + [\lambda_\Phi(t) - p]\} \phi_1 - q \phi_1, \end{aligned} \quad (19)$$

$$\begin{aligned} \partial_t \phi_0 = & -[H + \beta_n n + \beta_s(n_1 + n_{-1})] \phi_0 \\ & - 2\beta_s \phi_{-1} \bar{\phi}_0 \phi_1 + \mu_\Phi(t) \phi_0, \end{aligned} \quad (20)$$

$$\begin{aligned} \partial_t \phi_{-1} = & -[H + \beta_n n + \beta_s(n_{-1} + n_0 - n_1)] \phi_{-1} - \beta_s \phi_0^2 \bar{\phi}_1 \\ & + \{\mu_\Phi(t) - [\lambda_\Phi(t) - p]\} \phi_{-1} - q \phi_{-1}, \end{aligned} \quad (21)$$

where $\mu_\Phi(t)$ and $\lambda_\Phi(t)$ are functionals of $\Phi = (\phi_1, \phi_0, \phi_{-1})^T$ and they are chosen such that the above CNGF is mass (or normalization) and magnetization conserved. The CNGF can be proven to be energy diminishing for any given initial data. The linear Zeeman term p is grouped together with λ_Φ , acting as a Lagrange multiplier in the energy minimization process. A first-order time-splitting scheme will be applied to the CNGF (19)–(21), to form the standard normalized gradient flow for ground-state computation, as well as to find the third normalization condition. There are two ways to deal with the quadratic Zeeman energy q during the time-splitting procedure, and we call the two numerical treatments as projection with a magnetic field (PWMF) and projection without a magnetic field (POMF), respectively.

A. Projection with a magnetic field

The first way to deal with the Zeeman energy is to apply a first-order time splitting to the CNGF (19)–(21) in discrete time interval $t_{n-1} \leq t \leq t_n$, where $t_n = n\Delta t$ with time step Δt , in the following way.

Step 1:

$$\partial_t \phi_1 = -[H + \beta_n n + \beta_s(n_1 + n_0 - n_{-1})] \phi_1 - \beta_s \bar{\phi}_{-1} \phi_0^2, \quad (22)$$

$$\partial_t \phi_0 = -[H + \beta_n n + \beta_s(n_1 + n_{-1})] \phi_0 - 2\beta_s \phi_{-1} \bar{\phi}_0 \phi_1, \quad (23)$$

$$\partial_t \phi_{-1} = -[H + \beta_n n + \beta_s(n_{-1} + n_0 - n_1)] \phi_{-1} - \beta_s \phi_0^2 \bar{\phi}_1. \quad (24)$$

Step 2:

$$\partial_t \phi_1(\mathbf{x}, t) = \{\mu_\Phi(t) + [\lambda_\Phi(t) - p]\} \phi_1 - q \phi_1, \quad (25)$$

$$\partial_t \phi_0(\mathbf{x}, t) = \mu_\Phi(t) \phi_0, \quad t_{n-1} \leq t \leq t_n, \quad (26)$$

$$\partial_t \phi_{-1}(\mathbf{x}, t) = \{\mu_\Phi(t) - [\lambda_\Phi(t) - p]\} \phi_{-1} - q \phi_{-1}. \quad (27)$$

The nonlinear ordinary differential equations (ODEs) (25)–(27) are equivalent to the projection step

$$\phi_1(\mathbf{x}, t_n) := \phi_1(\mathbf{x}, t_n^+) = \sigma_1^n \phi_1(\mathbf{x}, t_n^-), \quad (28)$$

$$\phi_0(\mathbf{x}, t_n) := \phi_0(\mathbf{x}, t_n^+) = \sigma_0^n \phi_0(\mathbf{x}, t_n^-), \quad (29)$$

$$\phi_{-1}(\mathbf{x}, t_n) := \phi_{-1}(\mathbf{x}, t_n^+) = \sigma_{-1}^n \phi_{-1}(\mathbf{x}, t_n^-), \quad (30)$$

where $\phi_l(\mathbf{x}, t_n^\pm) = \lim_{t \rightarrow t_n^\pm} \phi_l(\mathbf{x}, t)$ ($l = -1, 0, 1$) and σ_l^n ($l = -1, 0, 1$) are the normalization constants. From the solution of the nonlinear ODEs (25)–(27), a third normalization condition for the normalization constants can be derived as (see derivation in Appendix A)

$$\sigma_1^n \sigma_{-1}^n = e^{-2q\Delta t} (\sigma_0^n)^2. \quad (31)$$

Together with the two physical conditions on the conservation of mass and conservation of magnetization, it determines the three normalization constants as (see details in Appendix A)

$$\sigma_0^n = \frac{\sqrt{1-M^2}}{[N_0^- + \sqrt{4e^{-4q\Delta t}(1-M^2)N_1^-N_{-1}^- + (MN_0^-)^2}]^{1/2}}, \quad (32)$$

$$\sigma_1^n = \sqrt{\frac{1+M - (\sigma_0^n)^2 N_0^-}{2N_1^-}}, \quad (33)$$

$$\sigma_{-1}^n = \sqrt{\frac{1-M - (\sigma_0^n)^2 N_0^-}{2N_{-1}^-}}, \quad (34)$$

where $N_l^- = \|\phi_l(\cdot, t_n^-)\|^2$ ($l = -1, 0, 1$), with $\phi_l(\cdot, t_n^-)$ ($l = -1, 0, 1$) being the solution of (22)–(24) at $t = t_n^-$.

B. Projection without a magnetic field

Another approach to deal with the magnetic field is to retain q in the gradient flow equations instead of including it in the normalization step. This yields the gradient flow (step 1)

$$\partial_t \phi_1 = -[H + \beta_n n + \beta_s(n_1 + n_0 - n_{-1})] \phi_1 - \beta_s \bar{\phi}_{-1} \phi_0^2 - q \phi_1, \quad (35)$$

$$\partial_t \phi_0 = -[H + \beta_n n + \beta_s(n_1 + n_{-1})] \phi_0 - 2\beta_s \phi_{-1} \bar{\phi}_0 \phi_1, \quad (36)$$

$$\partial_t \phi_{-1} = -[H + \beta_n n + \beta_s(n_{-1} + n_0 - n_1)] \phi_{-1} - \beta_s \phi_0^2 \bar{\phi}_1 - q \phi_{-1}, \quad (37)$$

and the ODEs (step 2)

$$\partial_t \phi_1(\mathbf{x}, t) = \{\mu_\Phi(t) + [\lambda_\Phi(t) - p]\} \phi_1, \quad (38)$$

$$\partial_t \phi_0(\mathbf{x}, t) = \mu_\Phi(t) \phi_0, \quad t_{n-1} \leq t \leq t_n, \quad (39)$$

$$\partial_t \phi_{-1}(\mathbf{x}, t) = \{\mu_\Phi(t) - [\lambda_\Phi(t) - p]\} \phi_{-1}, \quad (40)$$

which are equivalent to projection steps (28)–(30). The normalization constants in this case are given by [26]

$$\sigma_0^n = \frac{\sqrt{1-M^2}}{[N_0^- + \sqrt{4(1-M^2)N_1^-N_{-1}^- + (MN_0^-)^2}]^{1/2}}, \quad (41)$$

$$\sigma_1^n = \sqrt{\frac{1+M - (\sigma_0^n)^2 N_0^-}{2N_1^-}}, \quad (42)$$

$$\sigma_{-1}^n = \sqrt{\frac{1-M - (\sigma_0^n)^2 N_0^-}{2N_{-1}^-}}. \quad (43)$$

In fact, when $q=0$, the derivation of (32)–(34) collapses to the one for (41)–(43).

IV. NUMERICAL COMPARISON

In this section, we compute the ground state of a spin-1 BEC confined in a cigar-shaped harmonic oscillator potential and perform a comparison between the accuracy of the ground-state solution obtained via the PWMF and POMF methods. The atoms are tightly confined in two directions and can be effectively described by one-dimensional (1D) CGPEs. Both gradient flows (22)–(24) and (35)–(37) can be discretized by the backward-forward Euler sine-pseudo-spectral (BFSP) method, which was designed to effectively solve for the single-component BEC ground state [25]. However, in order to obtain a complete comparison between different numerical schemes, we apply also the backward Euler sine-pseudospectral (BESP) discretization [25] to the two gradient flows. Thus two different projections—i.e., PWMF and POMF—and two different discretizations—i.e., BFSP and BESP—give four combinations of numerical schemes:

- (i) PWMF+BFSP,
- (ii) PWMF+BESP,
- (iii) POMF+BFSP,
- (iv) POMF+BESP.

In the following, we will compare the accuracy and efficiency of the four schemes. Numerical results obtained using different time steps are compared to the estimated exact solutions, which are obtained using time step $\Delta t = 5 \times 10^{-5}$. For the parameter sets we used, all four numerical schemes give the same results under this time step. In studying the numerical accuracy, we use the following notation to indicate the numerical errors: $\epsilon_{N_1}^{\Delta t}$, error in the fractional mass of spin component $m_F=1$ computed with time step Δt , and $\epsilon_E^{\Delta t}$, error in the total energy computed with time step Δt .

For the reference to the readers, the details of BFSP discretization of the POMF method are attached in Appendix B and it can be easily generalized to the rest of the numerical schemes.

A. Ferromagnetic interaction

For the case of a condensate with ferromagnetic interaction, we consider 10^4 ^{87}Rb atoms in a cigar-shaped harmonic potential with trapping frequencies $\omega_x = 2\pi \times 20$ Hz and $\omega_y = \omega_z = 2\pi \times 400$ Hz. The atomic parameters are given by $m = 86.909$ u, $a_0 = 5.387$ nm, $a_2 = 5.313$ nm, and $E_{\text{hfs}} = 4.5287 \times 10^{-24}$ J. The uniform magnetic field B (G) is applied in the z direction, and the effective one-dimensional potential and parameters are found to be $V(x) = \frac{1}{2}x^2$, $\beta_n = \frac{2(a_0+2a_2)N\sqrt{\omega_x\omega_z}}{3a_s\omega_x} = 885.4$, $\beta_s = \frac{2(a_2-a_0)N\sqrt{\omega_x\omega_z}}{3a_s\omega_x} = -4.1$, $p = -34\,990.6346B$, and $q = 3.5827B^2$, where the dimensionless length scaling unit a_s

TABLE I. Comparison of different numerical schemes for computing the spin-1 ^{87}Rb ground state in a uniform magnetic field with Zeeman energies $p=5845.80$ and $q=0.5$ (the smallest error is underlined).

	Method	$\epsilon_{N_1}^{0.01}$	$\epsilon_E^{0.01}$	$\epsilon_{N_1}^{0.001}$	$\epsilon_E^{0.001}$
$M=0.2$	PWMF+BFSP	0.018	0.0006	0.002	0.0001
	PWMF+BESP	<u>0.007</u>	<u>0</u>	<u>0.001</u>	0.0001
$N_1=0.306$ $E=-1132.9770$	POMF+BFSP	0.015	0.0005	0.003	0
	POMF+BESP	0.015	0.0005	0.002	0
$M=0.5$	PWMF+BFSP	0.007	0.0002	0.001	0.0001
	PWMF+BESP	<u>0.004</u>	<u>0.0001</u>	<u>0</u>	0.0001
$N_1=0.535$ $E=-2886.7040$	POMF+BFSP	0.007	0.0004	0.001	0.0001
	POMF+BESP	0.015	0.0013	0.002	0.0001
$M=0.8$	PWMF+BFSP	<u>0.001</u>	0.0002	0	0.0001
	PWMF+BESP	0.003	<u>0.0001</u>	0	0.0001
$N_1=0.805$ $E=-4640.4221$	POMF+BFSP	<u>0.001</u>	0.0002	0	0.0001
	POMF+BESP	0.005	0.0009	0	0.0001

$=2.4116 \mu\text{m}$ and time scaling unit $t_s=7.958$ ms.

Tables I and II compare the accuracy of different numerical schemes in computing the spin-1 ^{87}Rb ground state in a uniform magnetic field $B=1.6707 \times 10^{-1}$ G ($p=5845.80$, $q=0.5$) and $B=3.7357 \times 10^{-1}$ G ($p=13071.61$, $q=0.5$), respectively. As shown in the two tables, scheme 2—i.e., PWMF with BESP discretization—gives the most accurate results under a large time step ~ 0.01 . When a smaller time step—e.g., $\Delta t \sim 0.001$ —is used, all four numerical schemes give good results. In terms of efficiency, the BFSP method is preferable in the case of a smaller time step since it is explicit.

B. Antiferromagnetic interaction

For the case of condensate with antiferromagnetic interaction, we consider 10^4 ^{23}Na atoms in the cigar-shaped harmonic potential with trapping frequencies $\omega_x=2\pi \times 20$ Hz

and $\omega_y=\omega_z=2\pi \times 400$ Hz. The atomic parameters are $m=22.99$ u, $a_0=2.646$ nm, $a_2=2.911$ nm, and $E_{\text{hfs}}=1.1739 \times 10^{-24}$ J. The effective one-dimensional potential and parameters are found to be $V(x)=\frac{1}{2}x^2$, $\beta_n=240.8$, $\beta_s=7.5$, $p=34\,990.6346B$, and $q=13.8216B^2$, where the dimensionless length scaling unit $a_s=4.6896 \mu\text{m}$ and time scaling unit $t_s=7.958$ ms.

Tables III and IV compare the accuracy of different numerical schemes in computing the spin-1 ^{23}Na ground state in a uniform magnetic field $B=8.5059 \times 10^{-2}$ G ($p=2976.27$, $q=0.5$) and $B=1.9020 \times 10^{-1}$ G ($p=13071.61$, $q=0.5$), respectively. From the two tables, numerical scheme 3—i.e., POMF with BFSP discretization—always gives the results with the smallest error, in particular the case when the total magnetization is close to the critical magnetization, which will be discussed later. Therefore, we conclude that the POMF method with BFSP discretization is the best for

 TABLE II. Comparison of different numerical schemes for computing the spin-1 ^{87}Rb ground state in a uniform magnetic field with Zeeman energies $p=13071.61$ and $q=0.5$ (the smallest error is underlined).

	Method	$\epsilon_{N_1}^{0.01}$	$\epsilon_E^{0.01}$	$\epsilon_{N_1}^{0.001}$	$\epsilon_E^{0.001}$
$M=0.2$	PWMF+BFSP	0.006	0.0009	0.001	0
	PWMF+BESP	<u>0.002</u>	<u>0.0001</u>	<u>0</u>	0
$N_1=0.211$ $E=-2578.0254$	POMF+BFSP	0.014	0.0025	0.002	0
	POMF+BESP	0.014	0.0024	0.001	0
$M=0.5$	PWMF+BFSP	0.002	0.0005	0	0.0001
	PWMF+BESP	<u>0</u>	<u>0.0001</u>	0	0
$N_1=0.505$ $E=-6499.3979$	POMF+BFSP	0.004	0.0008	0.001	0.0001
	POMF+BESP	0.007	0.0017	0.001	0.0001
$M=0.8$	PWMF+BFSP	0	0.0002	0	0
	PWMF+BESP	0	<u>0.0001</u>	0	0
$N_1=0.801$ $E=-10420.7489$	POMF+BFSP	0	0.0002	0	0
	POMF+BESP	0.001	0.0005	0	0

TABLE III. Comparison of different numerical schemes for computing the spin-1 ^{23}Na ground state in a uniform magnetic field with Zeeman energies $p=2976.27$ and $q=0.1$ (the smallest error is underlined).

	Method	$\epsilon_{N_1}^{0.01}$	$\epsilon_E^{0.01}$	$\epsilon_{N_1}^{0.001}$	$\epsilon_E^{0.001}$
$M=0.2$	PWMF+BFSP	0.022	0.0008	0.003	0
	PWMF+BESP	0.03	0.0012	0.005	0
$N_1=0.277$ $E=-579.9371$	POMF+BFSP	<u>0.007</u>	<u>0.0002</u>	<u>0.001</u>	0
	POMF+BESP	0.046	0.0022	0.007	0
$M=0.55$	PWMF+BFSP	0.072	0.0032	0.034	0.0002
	PWMF+BESP	0.092	0.0057	0.026	0.0005
$N_1=0.760$ $E=-1621.5122$	POMF+BFSP	<u>0.007</u>	<u>0.0001</u>	<u>0</u>	<u>0</u>
	POMF+BESP	0.081	0.0042	0.022	0.0003
$M=0.6$	PWMF+BFSP	0.052	0.0033	0.020	0.0009
	PWMF+BESP	0.085	0.0077	0.060	0.0042
$N_1=0.800$ $E=-1770.3084$	POMF+BFSP	<u>0</u>	<u>0.0001</u>	<u>0</u>	<u>0</u>
	POMF+BESP	0.074	0.0060	0.051	0.0031
$M=0.8$	PWMF+BFSP	0	0.0002	0	0.0001
	PWMF+BESP	0.004	0.0013	0	0.0001
$N_1=0.900$ $E=-2365.4656$	POMF+BFSP	0	<u>0.0001</u>	0	<u>0</u>
	POMF+BESP	0	0.0100	0	0.0100

computing the antiferromagnetic condensate ground state, for its high accuracy and efficiency in terms of computational time.

V. APPLICATIONS

The numerical solution of the spin-1 BEC ground state in a harmonic potential has been discussed in the literature [22]

by a different numerical method. In this section, we apply the POMF method with BFSP discretization to compute the spin-1 BEC ground state in a harmonic plus optical lattice potential. The ground-state solution in a harmonic potential is used as a reference frame to investigate the influence of the periodic potential, as well as the effect of interatomic interaction in the mean-field ground-state solution.

TABLE IV. Comparison of different numerical schemes for computing the spin-1 ^{23}Na ground state in a uniform magnetic field with Zeeman energies $p=6655.15$ and $q=0.5$ (the smallest error is underlined).

	Method	$\epsilon_{N_1}^{0.01}$	$\epsilon_E^{0.01}$	$\epsilon_{N_1}^{0.001}$	$\epsilon_E^{0.001}$
$M=0.2$	PWMF+BFSP	0.004	0.0008	0	0
	PWMF+BESP	0.005	0.0011	0	0
$N_1=0.209$ $E=-1315.6122$	POMF+BFSP	<u>0.001</u>	<u>0.0003</u>	0	0
	POMF+BESP	0.012	0.0037	0.001	0
$M=0.5$	PWMF+BFSP	0.009	0.0019	0.001	0.0001
	PWMF+BESP	<u>0.003</u>	<u>0.0003</u>	0	0
$N_1=0.522$ $E=-3311.9032$	POMF+BFSP	<u>0.003</u>	0.0004	0	0
	POMF+BESP	0.013	0.0020	0.001	0
$M=0.95$	PWMF+BFSP	0.012	0.0017	0.002	0
	PWMF+BESP	0.010	0.0012	0.002	0
$N_1=0.966$ $E=-6306.3645$	POMF+BFSP	0.006	<u>0.0002</u>	0.001	0
	POMF+BESP	<u>0.004</u>	<u>0.0002</u>	0	0
$M=0.99$	PWMF+BFSP	0.002	0.0006	0	0
	PWMF+BESP	0.001	0.0004	0	0
$N_1=0.995$ $E=-6572.5433$	POMF+BFSP	0	0.0001	0	0
	POMF+BESP	0	<u>0</u>	0	0

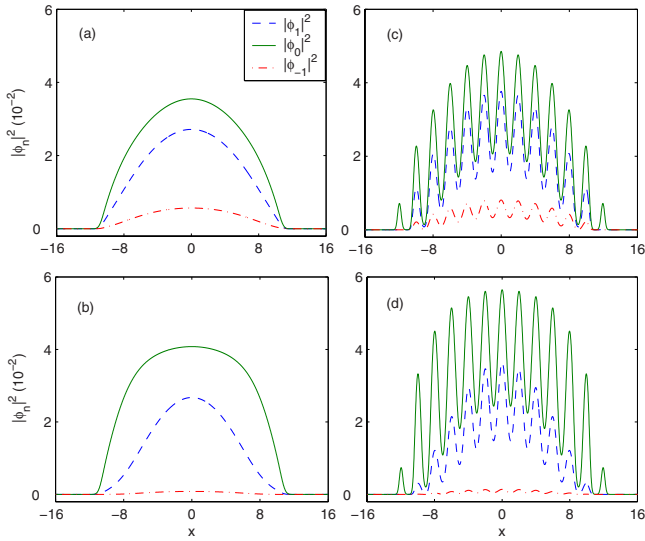


FIG. 1. (Color online) Ground state of ^{87}Rb with $M=0.3$ in a harmonic potential, (a) $q=0.1$, (b) $q=0.5$, and harmonic plus optical lattice potential, (c) $q=0.1$, (d) $q=0.5$.

A. Ferromagnetic interaction

Simulations for ^{87}Rb , with the same set of parameters as in Sec. IV A, are carried out for a harmonic plus optical lattice potential,

$$V(x) = \frac{1}{2}x^2 + V_0 \sin^2\left(\frac{\pi x}{2}\right), \quad (44)$$

where V_0 is the depth of the optical lattice. Figures 1(a) and 1(b) show the ground-state solutions of spin-1 ^{87}Rb ($M=0.3$) in the harmonic potential, while Figs. 1(c) and 1(d) show the ground-state solutions when the periodic potential with $V_0=50$ is added. The ground state in the potential (44) can be viewed as the ground state in a harmonic potential modulated by the periodic function. The relative population of each spinor component, as shown in Fig. 2, is found to be almost unaffected by the existence of the optical lattice except for the case of small magnetization.

We also investigated the effect of the spin-independent mean-field interaction—i.e., β_n —on the ground-state phase diagram. Figure 6, below, shows the relative population of each component for several β_n . The interaction is repulsive, and increasing β_n has the similar effect as increasing the magnitude of the magnetic field, or equivalently, increasing the quadratic Zeeman energy q .

B. Antiferromagnetic interaction

Simulations for ^{23}Na , with the same set of parameters as in Sec. IV B, are carried out for the harmonic plus optical lattice potential (44) with $V_0=50$. Figures 3(a) and 3(b) show the ground-state solutions of spin-1 ^{23}Na ($M=0.3$) in a harmonic potential, while Figs. 3(c) and 3(d) show the solutions when the periodic potential exists. For both potentials, ϕ_0 is immiscible with ϕ_1 and ϕ_{-1} . For constant M , the immiscibility property is better defined for larger q , with thinner overlapping layers. In the existence of a periodic potential,

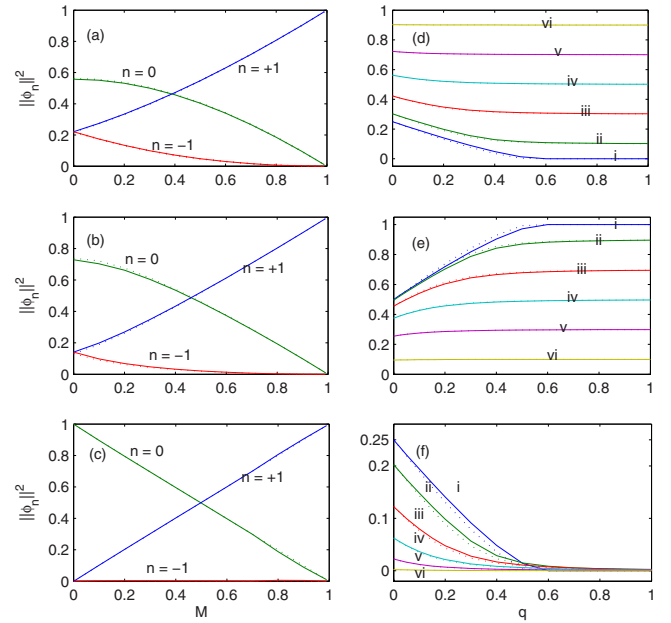


FIG. 2. (Color online) (Left) Relative population of each hyperfine component of ^{87}Rb in a harmonic potential (dotted line) and a harmonic plus optical lattice potential (solid line), subjected to a magnetic field (a) $q=0.05$, (b) $q=0.2$, and (c) $q=1.0$. (Right) Relative population of each hyperfine component: (d) $m_F=+1$, (e) $m_F=0$, and (f) $m_F=-1$ of ^{87}Rb in a harmonic potential (dotted line) and a harmonic plus optical lattice potential (solid line), subjected to magnetic field $q=0.1$, for (i) $M=0$, (ii) $M=0.1$, (iii) $M=0.3$, (iv) $M=0.5$, (v) $M=0.7$, and (vi) $M=0.9$.

the immiscibility property of the three components is further enhanced.

Figure 4 depicts the relative population of each hyperfine component as a function of M and as a function of q , respectively. In the ground-state phase diagram of a condensate with antiferromagnetic interaction subjected to a weak magnetic field, there exists a critical value for magnetization

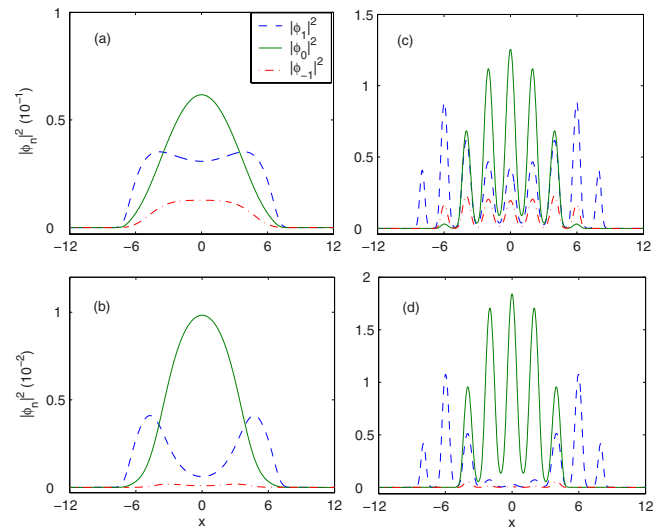


FIG. 3. (Color online) Ground state of ^{23}Na with $M=0.3$ in a harmonic potential, (a) $q=0.1$, (b) $q=0.5$, and harmonic plus optical lattice potential, (c) $q=0.1$, (d) $q=0.5$.

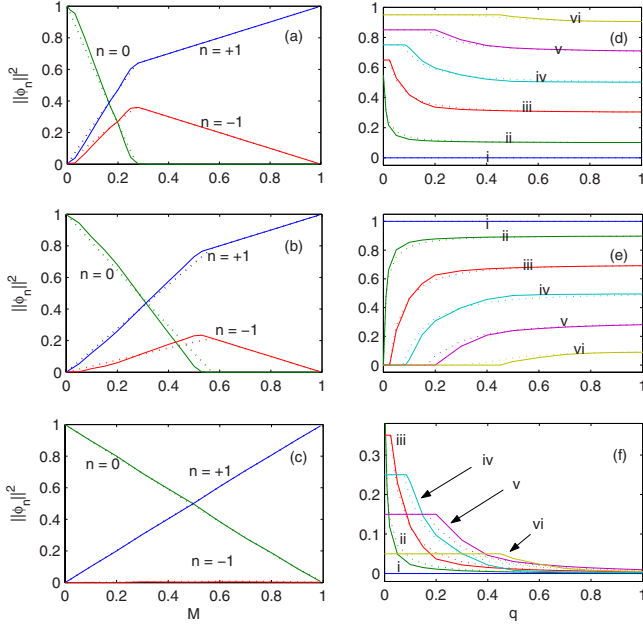


FIG. 4. (Color online) (Left) Relative population of each hyperfine component of ^{23}Na in a harmonic potential (dotted line) and a harmonic plus optical lattice potential (solid line), subjected to magnetic field, (a) $q=0.02$, (b) $q=0.1$, and (c) $q=1.0$. (Right) Relative population of each hyperfine component, (d) $m_F=+1$, (e) $m_F=0$, and (f) $m_F=-1$, of ^{23}Na in a harmonic potential (dotted line) and a harmonic plus optical lattice potential (solid line), subject to magnetic field $q=0.1$, for (i) $M=0$, (ii) $M=0.1$, (iii) $M=0.3$, (iv) $M=0.5$, (v) $M=0.7$, and (vi) $M=0.9$.

(M_c) such that when $M < M_c$, all three hyperfine components coexist, and when $M > M_c$, only components $m_F = \pm 1$ exist. At $M = M_c$, the ground state is not unique and two stationary solutions, one with the three coexisting components and the other one with zero particles in component $m_F=0$, share the same energy level. As shown in Fig. 4, the existence of an optical lattice has the effect of shifting M_c to a smaller value, or equivalently, shifting the critical value of magnetic field q_c to a larger value when M is held as constant. Computations are also carried out for an optical lattice of different depths V_0 in (44), and M_c as a function of q is plotted in Fig. 5. The critical magnetization M_c is found to decrease with increasing lattice depth.

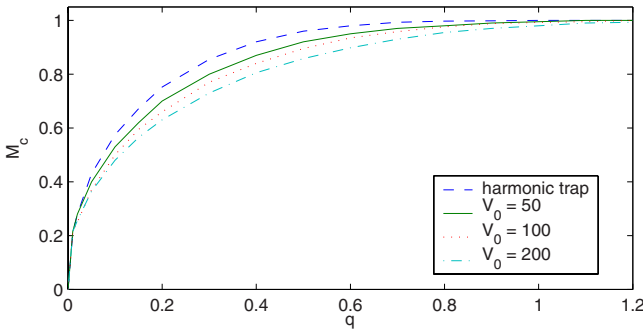


FIG. 5. (Color online) Variation of the critical magnetization M_c with respect to the quadratic Zeeman energy q for 10^4 spin-1 ^{23}Na atoms in different trapping potentials.

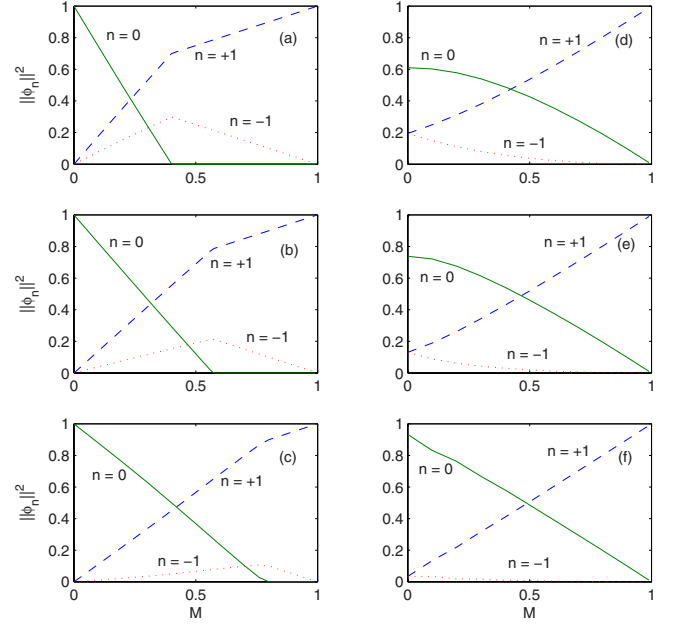


FIG. 6. (Color online) Relative population of each hyperfine component of (left) ^{23}Na with $\beta_s=7.5$ and (a) $\beta_n=24.08$, (b) $\beta_n=240.8$, and (c) $\beta_n=2408$ and of (right) ^{87}Rb with $\beta_s=-4.1$ and (d) $\beta_n=88.54$, (e) $\beta_n=885.4$, and (f) $\beta_n=8854$, in harmonic potential $V(x)=\frac{1}{2}x^2$.

The effect of the spin-independent mean-field interaction on the ground-state phase diagram is also investigated for the antiferromagnetic interaction case. Figure 6 shows the relative population of each component for several β_n . The same as the ferromagnetic case, increasing β_n has a similar effect as increasing the magnitude of the magnetic field. A large β_n gives a larger critical magnetization. The relation between M_c and β_n is depicted in Fig. 7.

VI. CONCLUSION

In this paper, we proposed a method of normalized gradient flow to compute the ground state of spin-1 Bose-Einstein condensates in a uniform magnetic field. Using a similar approach as the normalized gradient flow for computing the spin-1 condensate ground state without an external magnetic

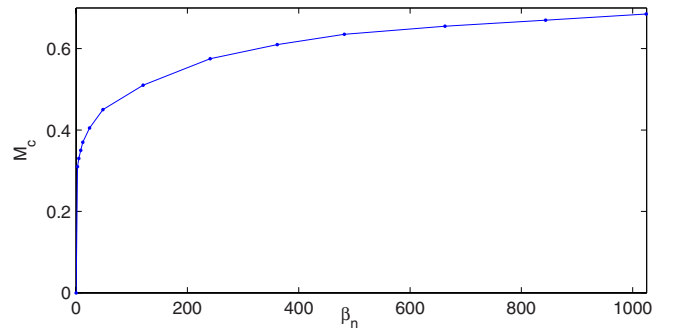


FIG. 7. (Color online) Variation of the critical magnetization M_c with respect to the spin-independent mean-field interaction β_n for spin-1 ^{23}Na atoms with spin-exchange interaction $\beta_s=7.5$.

field, we found two ways to incorporate the Zeeman energies with the coupled Gross-Pitaevskii equations numerically: (i) The PWMF method (both linear and quadratic Zeeman terms are treated in the normalization step) and (ii) POMF method (the quadratic Zeeman term is retained in the gradient flow while the linear Zeeman term is included in the normalization step). In both treatments, the effect of the linear Zeeman term will finally be canceled out in the third normalization condition and it has no effect on the ground-state solution. Numerical results show that the POMF approach with the backward-forward Euler sine-pseudospectral method is the best numerical scheme for the ground-state computation, in terms of accuracy and efficiency.

The condensate ground state in a harmonic plus optical lattice potential, for the cases of different quadratic Zeeman energies, is also studied. For a condensate with ferromagnetic interaction, the existence of an optical lattice makes no significant difference in the ground-state phase diagram except for small M , as compared to the condensate ground state in a harmonic trap. For a condensate with antiferromagnetic interaction, the optical lattice tends to reduce the critical value of the magnetization M_c and M_c can be further reduced by increasing the lattice depth.

ACKNOWLEDGMENTS

This work is supported by Singapore Ministry of Education Grant No. R-158-000-002-112. The work was partially done while the authors were visiting the Institute for Mathematical Sciences of the National University of Singapore.

APPENDIX A: DERIVATION OF THE NORMALIZATION CONSTANTS FOR THE PWMF METHOD

The solutions of the nonlinear ODEs (25)–(27) can be expressed as

$$\phi_1^n = \exp\left(\int_{t_{n-1}}^{t_n} [\mu_\Phi + \lambda_\Phi - p - q] d\tau\right) \phi_1^{n-1}, \quad (\text{A1})$$

$$\phi_0^n = \exp\left(\int_{t_{n-1}}^{t_n} \mu_\Phi d\tau\right) \phi_0^{n-1}, \quad (\text{A2})$$

$$\phi_{-1}^n = \exp\left(\int_{t_{n-1}}^{t_n} [\mu_\Phi - \lambda_\Phi + p - q] d\tau\right) \phi_{-1}^{n-1}, \quad (\text{A3})$$

where $\phi_l^n = \phi_l(\mathbf{x}, t_n)$. This solution suggests the following relation between the three exponential terms:

$$\begin{aligned} & \exp\left(\int_{t_{n-1}}^{t_n} [\mu_\Phi(\tau) + \lambda_\Phi(\tau) - p - q] d\tau\right) \\ & \times \exp\left(\int_{t_{n-1}}^{t_n} [\mu_\Phi(\tau) - \lambda_\Phi(\tau) + p - q] d\tau\right) \\ & = \exp\left(\int_{t_{n-1}}^{t_n} [2\mu_\Phi(\tau) - 2q] d\tau\right) \\ & = e^{-2q\Delta t} \left[\exp\left(\int_{t_{n-1}}^{t_n} \mu_\Phi(\tau) d\tau\right) \right]^2. \end{aligned} \quad (\text{A4})$$

The three exponential terms play the same roles as the normalization constants σ_l^n ($l=1, 0, -1$) and therefore immediately suggest the third normalization condition (31). This, together with the two existing physical constraints on the total mass and total magnetization,

$$\sum_{l=-1}^1 (\sigma_l^n)^2 \|\phi_l(\cdot, t_n^-)\|^2 = 1, \quad (\text{A5})$$

$$(\sigma_1^n)^2 \|\phi_1(\cdot, t_n^-)\|^2 - (\sigma_{-1}^n)^2 \|\phi_{-1}(\cdot, t_n^-)\|^2 = M, \quad (\text{A6})$$

determines uniquely the normalization constants σ_l^n ($l=1, 0, -1$) in (28)–(30). Let $N_l^- = \|\phi_l(\cdot, t_n^-)\|^2$ ($l=-1, 0, 1$) and summing (A5) and (A6), we get

$$2(\sigma_1^n)^2 N_1^- = 1 + M - (\sigma_0^n)^2 N_0^-. \quad (\text{A7})$$

This immediately implies

$$\sigma_1^n = \sqrt{\frac{1 + M - (\sigma_0^n)^2 N_0^-}{2N_1^-}}. \quad (\text{A8})$$

Subtracting (A6) from (A5), we obtain

$$2(\sigma_{-1}^n)^2 N_{-1}^- = 1 - M - (\sigma_0^n)^2 N_0^-. \quad (\text{A9})$$

Again, this immediately implies

$$\sigma_{-1}^n = \sqrt{\frac{1 - M - (\sigma_0^n)^2 N_0^-}{2N_{-1}^-}}. \quad (\text{A10})$$

Multiplying (A8) and (A10) and noticing (31), we get

$$[1 + M - (\sigma_0^n)^2 N_0^-][1 - M - (\sigma_0^n)^2 N_0^-] = 4e^{-4q\Delta t} N_{-1}^- N_1^- (\sigma_0^n)^4. \quad (\text{A11})$$

Simplifying the above equation, we obtain

$$[(N_0^-)^2 - 4e^{-4q\Delta t} N_{-1}^- N_1^-] (\sigma_0^n)^4 - 2N_0^- (\sigma_0^n)^2 + (1 - M^2) = 0. \quad (\text{A12})$$

Solving the above equation and noticing $(\sigma_0^n)^2 N_0^- \ll (1 - M^2)$, we get

$$\begin{aligned} (\sigma_0^n)^2 &= \frac{N_0^- - \sqrt{4e^{-4q\Delta t} (1 - M^2) N_{-1}^- N_1^- + M^2 (N_0^-)^2}}{(N_0^-)^2 - 4N_{-1}^- N_1^-} \\ &= \frac{1 - M^2}{N_0^- + \sqrt{4e^{-4q\Delta t} (1 - M^2) N_{-1}^- N_1^- + M^2 (N_0^-)^2}}. \end{aligned} \quad (\text{A13})$$

Thus it immediately implies the solution in (32).

APPENDIX B: BFSP DISCRETIZATION FOR THE POMF METHOD

We present here the BESF method to discretize the normalized gradient flow (35)–(37) and (28)–(30). As the trapping potential $V(\mathbf{x})$ grows to infinity at far field, the solution $\Phi(\mathbf{x}, t)$ decays to zero exponentially fast when $|\mathbf{x}| \rightarrow \infty$. Thus we truncate the problem into a bounded computational domain $\Omega_{\mathbf{x}}$ [chosen as an interval (a, b) in 1D, a rectangle

$(a, b) \times (c, d)$ in 2D, and a box $(a, b) \times (c, d) \times (e, f)$ in 3D, with $|a|, |c|, |e|, b, d,$ and f sufficiently large] with homogeneous Dirichlet boundary conditions.

For simplicity of notation we shall introduce the method for the case of one spatial dimension ($d=1$) defined over the interval (a, b) with homogeneous Dirichlet boundary conditions. Generalization to higher dimension is straightforward for tensor product grids, and the results remain valid without modifications. For $d=1$, we choose the spatial mesh size $h = \Delta x > 0$ with $h=(b-a)/L$, with L being an even positive integer, and let the grid points be

$$x_j := a + jh, \quad j = 0, 1, \dots, L.$$

Let $\Phi_j^n = (\phi_{1,j}^n, \phi_{0,j}^n, \phi_{-1,j}^n)^T$ be the approximation of $\Phi(x_j, t_n) = (\phi_1(x_j, t_n), \phi_0(x_j, t_n), \phi_{-1}(x_j, t_n))^T$ and Φ^n be the solution vector with component Φ_j^n . In the discretization, we use the sine-pseudospectral method for spatial derivatives and backward (forward) Euler scheme for linear (nonlinear) terms in time discretization. The gradient flow (35)–(37) is discretized, for $j=1, 2, \dots, L-1$ and $n \geq 1$, as

$$\frac{\phi_{1,j}^* - \phi_{1,j}^{n-1}}{\Delta t} = \frac{1}{2} D_{xx}^s \phi_{1,j}^* |x_j - (\alpha_1 + q) \phi_{1,j}^* + G_{1,j}^{n-1}, \quad (\text{B1})$$

$$\frac{\phi_{0,j}^* - \phi_{0,j}^{n-1}}{\Delta t} = \frac{1}{2} D_{xx}^s \phi_{0,j}^* |x_j - \alpha_0 \phi_{0,j}^* + G_{0,j}^{n-1}, \quad (\text{B2})$$

$$\frac{\phi_{-1,j}^* - \phi_{-1,j}^{n-1}}{\Delta t} = \frac{1}{2} D_{xx}^s \phi_{-1,j}^* |x_j - (\alpha_{-1} + q) \phi_{-1,j}^* + G_{-1,j}^{n-1}, \quad (\text{B3})$$

where

$$G_{1,j}^{n-1} = [\alpha_1 - V(x_j) - (\beta_n + \beta_s)(|\phi_{1,j}^{n-1}|^2 + |\phi_{0,j}^{n-1}|^2) - (\beta_n - \beta_s)|\phi_{-1,j}^{n-1}|^2] \phi_{1,j}^{n-1} - \beta_s \bar{\phi}_{-1,j}^{n-1} (\phi_{0,j}^{n-1})^2,$$

$$G_{0,j}^{n-1} = [\alpha_0 - V(x_j) - (\beta_n + \beta_s)(|\phi_{1,j}^{n-1}|^2 + |\phi_{-1,j}^{n-1}|^2) - \beta_n |\phi_{0,j}^{n-1}|^2] \phi_{0,j}^{n-1} - 2\beta_s \phi_{-1,j}^{n-1} \bar{\phi}_{0,j}^{n-1} \phi_{1,j}^{n-1},$$

$$G_{-1,j}^{n-1} = [\alpha_{-1} - V(x_j) - (\beta_n + \beta_s)(|\phi_{-1,j}^{n-1}|^2 + |\phi_{0,j}^{n-1}|^2) - (\beta_n - \beta_s)|\phi_{1,j}^{n-1}|^2] \phi_{-1,j}^{n-1} - \beta_s (\phi_{0,j}^{n-1})^2 \bar{\phi}_{1,j}^{n-1}.$$

Here, D_{xx}^s , a pseudospectral differential operator approximation of ∂_{xx} , is defined as

$$D_{xx}^s U|_{x=x_j} = - \sum_{m=1}^{L-1} \mu_m^2 (\hat{U})_m \sin[\mu_m(x_j - a)],$$

$$j = 1, 2, \dots, L-1,$$

where $(\hat{U})_m$ ($m=1, 2, \dots, L-1$), the sine transform coefficients of the vector $U = (U_0, U_1, \dots, U_L)^T$ satisfying $U_0 = U_L = 0$, are defined as

$$\mu_m = \frac{\pi m}{b-a},$$

$$(\hat{U})_m = \frac{2}{L} \sum_{j=1}^{L-1} U_j \sin[\mu_m(x_j - a)], \quad m = 1, 2, \dots, L-1,$$

and α_l ($l=-1, 0, 1$) are the stabilization parameters which are chosen in the optimal form (such that the time step can be chosen as large as possible) as [25]

$$\alpha_l = \frac{1}{2} (b_l^{\max} + b_l^{\min}), \quad l = -1, 0, 1, \quad (\text{B4})$$

with

$$b_1^{\max} = \max_{1 \leq j \leq L-1} [V(x_j) + (\beta_n + \beta_s)(|\phi_{1,j}^{n-1}|^2 + |\phi_{0,j}^{n-1}|^2) + (\beta_n - \beta_s)|\phi_{-1,j}^{n-1}|^2],$$

$$b_1^{\min} = \min_{1 \leq j \leq L-1} [V(x_j) + (\beta_n + \beta_s)(|\phi_{1,j}^{n-1}|^2 + |\phi_{0,j}^{n-1}|^2) + (\beta_n - \beta_s)|\phi_{-1,j}^{n-1}|^2],$$

$$b_0^{\max} = \max_{1 \leq j \leq L-1} [V(x_j) + (\beta_n + \beta_s)(|\phi_{1,j}^{n-1}|^2 + |\phi_{-1,j}^{n-1}|^2) + \beta_n |\phi_{0,j}^{n-1}|^2],$$

$$b_0^{\min} = \min_{1 \leq j \leq L-1} [V(x_j) + (\beta_n + \beta_s)(|\phi_{1,j}^{n-1}|^2 + |\phi_{-1,j}^{n-1}|^2) + \beta_n |\phi_{0,j}^{n-1}|^2],$$

$$b_{-1}^{\max} = \max_{1 \leq j \leq L-1} [V(x_j) + (\beta_n + \beta_s)(|\phi_{-1,j}^{n-1}|^2 + |\phi_{0,j}^{n-1}|^2) + (\beta_n - \beta_s)|\phi_{1,j}^{n-1}|^2],$$

$$b_{-1}^{\min} = \min_{1 \leq j \leq L-1} [V(x_j) + (\beta_n + \beta_s)(|\phi_{-1,j}^{n-1}|^2 + |\phi_{0,j}^{n-1}|^2) + (\beta_n - \beta_s)|\phi_{1,j}^{n-1}|^2].$$

The homogeneous Dirichlet boundary conditions are discretized as

$$\phi_{1,0}^* = \phi_{1,L}^* = \phi_{0,0}^* = \phi_{0,L}^* = \phi_{-1,0}^* = \phi_{-1,L}^* = 0. \quad (\text{B5})$$

The projection step (28)–(30) is discretized, for $0 \leq j \leq L$ and $n \geq 1$, as

$$\phi_{l,j}^n = \sigma_l^n \phi_{l,j}^*, \quad l = -1, 0, 1, \quad (\text{B6})$$

where

$$\sigma_0^n = \frac{\sqrt{1-M^2}}{[\|\phi_0^*\|^2 + \sqrt{4(1-M^2)}\|\phi_1^*\|^2\|\phi_{-1}^*\|^2 + M^2\|\phi_0^*\|^4]^{1/2}}, \quad (\text{B7})$$

$$\sigma_1^n = \frac{\sqrt{1+M-\alpha_0^2\|\phi_0^*\|^2}}{\sqrt{2}\|\phi_1^*\|}, \quad \sigma_{-1}^n = \frac{\sqrt{1-M-\alpha_0^2\|\phi_0^*\|^2}}{\sqrt{2}\|\phi_{-1}^*\|}, \quad (\text{B8})$$

with

$$\|\phi_l^*\|^2 = h \sum_{j=1}^{L-1} |\phi_{l,j}^*|^2, \quad l = -1, 0, 1.$$

The linear system (B1)–(B3) can be solved very efficiently by using the fast sine transform. In fact, taking the discrete sine transform at both sides and solving the system in phase space, we obtain

$$(\hat{\phi}_1^*)_m = \frac{(\hat{\phi}_1^{n-1})_m + (\hat{G}_1^{n-1})_m}{1 + \Delta t[q + \alpha_1 + \mu_m^2/2]}, \quad (\text{B9})$$

$$(\hat{\phi}_0^*)_m = \frac{(\hat{\phi}_0^{n-1})_m + (\hat{G}_0^{n-1})_m}{1 + \Delta t[\alpha_0 + \mu_m^2/2]}, \quad 1 \leq m < L, \quad (\text{B10})$$

$$(\hat{\phi}_{-1}^*)_m = \frac{(\hat{\phi}_{-1}^{n-1})_m + (\hat{G}_{-1}^{n-1})_m}{1 + \Delta t[q + \alpha_{-1} + \mu_m^2/2]}. \quad (\text{B11})$$

-
- [1] M. H. Anderson, J. R. Ensher, M. R. Matthews, C. E. Wieman, and E. A. Cornell, *Science* **269**, 198 (1995).
- [2] C. C. Bradley, C. A. Sackett, J. J. Tollett, and R. G. Hulet, *Phys. Rev. Lett.* **75**, 1687 (1995).
- [3] K. B. Davis, M. O. Mewes, M. R. Andrews, N. J. van Druten, D. S. Durfee, D. M. Kurn, and W. Ketterle, *Phys. Rev. Lett.* **75**, 3969 (1995).
- [4] E. P. Gross, *Nuovo Cimento* **20**, 454 (1961).
- [5] L. P. Pitaevskii, *Sov. Phys. JETP* **13**, 451 (1961).
- [6] F. Dalfovo, S. Giorgini, L. P. Pitaevskii, and S. Stringari, *Rev. Mod. Phys.* **71**, 463 (1999).
- [7] J. Stenger, S. Inouye, D. M. Stamper-Kurn, H.-J. Miesner, A. P. Chikkatur, and W. Ketterle, *Nature (London)* **396**, 345 (1998).
- [8] D. M. Stamper-Kurn, M. R. Andrews, A. P. Chikkatur, S. Inouye, H.-J. Miesner, J. Stenger, and W. Ketterle, *Phys. Rev. Lett.* **80**, 2027 (1998).
- [9] H. J. Miesner, D. M. Stamper-Kurn, J. Stenger, S. Inouye, A. P. Chikkatur, and W. Ketterle, *Phys. Rev. Lett.* **82**, 2228 (1999).
- [10] M. D. Barrett, J. A. Sauer, and M. S. Chapman, *Phys. Rev. Lett.* **87**, 010404 (2001).
- [11] B. J. Dabrowska-Wüster, E. A. Ostrovskaya, T. J. Alexander, and Y. S. Kivshar, *Phys. Rev. A* **75**, 023617 (2007).
- [12] A. Görlitz, T. L. Gustavson, A. E. Leanhardt, R. Löw, A. P. Chikkatur, S. Gupta, S. Inouye, D. E. Pritchard, and W. Ketterle, *Phys. Rev. Lett.* **90**, 090401 (2003).
- [13] T. L. Ho, *Phys. Rev. Lett.* **81**, 742 (1998).
- [14] T. Ohmi and K. Machida, *J. Phys. Soc. Jpn.* **67**, 1822 (1998).
- [15] C. V. Ciobanu, S. K. Yip, and T.-L. Ho, *Phys. Rev. A* **61**, 033607 (2000).
- [16] M. Ueda and M. Koashi, *Phys. Rev. A* **65**, 063602 (2002).
- [17] T. Mizushima, N. Kobayashi, and K. Machida, *Phys. Rev. A* **70**, 043613 (2004).
- [18] O. E. Müstecaplıoglu, M. Zhang, and L. You, *Phys. Rev. A* **71**, 053616 (2005).
- [19] M. Uchiyama, J. Ieda, and M. Wadati, *J. Phys. Soc. Jpn.* **75**, 064002 (2006).
- [20] J. Mur-Petit, M. Guilleumas, A. Polls, A. Sanpera, M. Lewenstein, K. Bongs, and K. Sengstock, *Phys. Rev. A* **73**, 013629 (2006).
- [21] K. Murata, H. Saito, and M. Ueda, *Phys. Rev. A* **75**, 013607 (2007).
- [22] W. Zhang, S. Yi, and L. You, *New J. Phys.* **5**, 77 (2003).
- [23] M. L. Chiofalo, S. Succi, and M. P. Tosi, *Phys. Rev. E* **62**, 7438 (2000).
- [24] W. Bao and Q. Du, *SIAM J. Sci. Comput. (USA)* **25**, 1674 (2004).
- [25] W. Bao, I.-L. Chern, and F. Y. Lim, *J. Comput. Phys.* **219**, 836 (2006).
- [26] W. Bao and F. Y. Lim, *SIAM J. Sci. Comput. (USA)* **30**, 1925 (2008).
- [27] H. Saito and M. Ueda, *Phys. Rev. A* **72**, 023610 (2005).
- [28] T. Isoshima and S. Yip, *J. Phys. Soc. Jpn.* **75**, 074605 (2006).
- [29] W. Bao and H. Wang, *SIAM (Soc. Ind. Appl. Math.) J. Numer. Anal.* **45**, 2177 (2007).